

Fast and slow precipitation responses to individual climate forcings: a PDRMIP multi-model study

Article

Accepted Version

Samset, B. H., Myhre, G., Forster, P. M., Hodnebrog, Ø., Andrews, T., Faluvegi, G., Fläschner, D., Kassoar, M., Kharin, V., Kirkevåg, A., Lamarque, J.-F., Olivié, D., Richardson, T., Shindell, D., Shine, K. P. ORCID: <https://orcid.org/0000-0003-2672-9978>, Takemura, T. and Voulgarakis, A. (2016) Fast and slow precipitation responses to individual climate forcings: a PDRMIP multi-model study. *Geophysical Research Letters*, 43 (6). pp. 2782-2791. ISSN 0094-8276 doi: 10.1002/2016GL068064 Available at <https://centaur.reading.ac.uk/63242/>

It is advisable to refer to the publisher's version if you intend to cite from the work. See [Guidance on citing](#).

Published version at: <http://dx.doi.org/10.1002/2016GL068064>

To link to this article DOI: <http://dx.doi.org/10.1002/2016GL068064>

Publisher: American Geophysical Union

Publisher statement: Green Open Access: AGU allows final articles to be placed in an institutional repository 6 months after publication, and allows submitted articles to be accessible on the author's personal website.

All outputs in CentAUR are protected by Intellectual Property Rights law,

including copyright law. Copyright and IPR is retained by the creators or other copyright holders. Terms and conditions for use of this material are defined in the [End User Agreement](#).

www.reading.ac.uk/centaur

CentAUR

Central Archive at the University of Reading

Reading's research outputs online

1 *Accepted version of Samset, B. H., et al. (2016), Fast and slow precipitation responses to individual climate*
2 *forcers: A PDRMIP multimodel study, Geophys. Res. Lett., 43, doi:10.1002/2016GL068064.*

3 **FAST AND SLOW PRECIPITATION RESPONSES TO INDIVIDUAL CLIMATE FORCERS: A PDRMIP MULTI-MODEL**
4 **STUDY**

5 B. H. Samset, CICERO Center for International Climate and Environmental Research – Oslo, Norway

6 G. Myhre, CICERO Center for International Climate and Environmental Research – Oslo, Norway

7 P. M. Forster, University of Leeds, Leeds, United Kingdom

8 Ø. Hodnebrog, CICERO Center for International Climate and Environmental Research – Oslo, Norway

9 T. Andrews, Met Office Hadley Centre, United Kingdom

10 G. Faluvegi, Columbia University, New York, USA

11 D. Fläschner, Max-Planck-Institut für Meteorologie, Hamburg, Germany

12 M. Kasoar, Imperial College London, London, United Kingdom

13 V. Kharin, Canadian Centre for Climate Modelling and Analysis, Gatineau, Canada

14 A. Kirkevåg, Norwegian Meteorological Institute, Oslo, Norway

15 J.-F. Lamarque, NCAR/UCAR, Boulder, USA

16 D. Olivié, Norwegian Meteorological Institute, Oslo, Norway

17 T. Richardson, University of Leeds, United Kingdom

18 D. Shindell, Duke University, Durham, USA

19 K. P. Shine, University of Reading, Reading, United Kingdom

T. Takemura, Kyushu University, Fukuoka, Japan

A. Voulgarakis, Imperial College London, London, United Kingdom

Abstract

Precipitation is expected to respond differently to various drivers of anthropogenic climate change. We present the first results from the Precipitation Driver and Response Model Intercomparison Project (PDRMIP), where nine global climate models have perturbed CO₂, CH₄, BC, sulfate and solar insolation. We divide the resulting changes to global mean and regional precipitation into fast responses that scale with changes in atmospheric absorption, and slow responses scaling with surface temperature change. While the overall features are broadly similar between models, we find significant regional inter-model variability, especially over land. Black carbon stands out as a component that may cause significant model diversity in predicted precipitation change. Processes linked to atmospheric absorption are less consistently modeled than those linked to top-of-atmosphere radiative forcing. We identify a number of land regions where the model ensemble consistently predicts that fast precipitation responses to climate perturbations dominate over the slow, temperature driven responses.

Key points

- Precipitation response from five climate drivers shown for nine climate models
- Fast responses scale with atmospheric absorption, slow with surface temperature
- Over some land regions, fast precipitation responses dominate the slow response

Introduction

Global precipitation levels and patterns are changing in response to global warming [Hartmann, 2013]. Climate change is presently caused by the interaction of drivers such as changing concentrations of

greenhouse gases, natural and anthropogenic aerosol emissions, and changes to solar insolation [Myhre *et al.*, 2013a]. While the connection between a changing temperature and the hydrological cycle may be understood through energy balance analyses [Allen and Ingram, 2002; O’Gorman *et al.*, 2012], future precipitation changes are poorly constrained in state of the art climate models [Collins *et al.*, 2013; Knutti and Sedláček, 2012]. Present models also tend to underestimate the solar absorption response to changes in water vapor following a climate perturbation, overestimating the resulting change in global mean precipitation [DeAngelis *et al.*, 2015]. Even when identically perturbed by an ensemble of climate forcings, differences in present models’ individual atmospheric responses to these forcings give rise to significant uncertainties. Improving such precipitation forecasts, both globally and regionally, and on short and long time scales, is an important topic in present climate research, since precipitation is one of the climate factors that most closely affects human society.

The global apparent hydrological sensitivity, defined as the total change in precipitation per degree of global warming, differs between climate drivers such as CO₂ and solar insolation [Allen and Ingram, 2002]. Further, the precipitation response to a climate forcing is usually thought to happen on two timescales: A rapid adjustment of the atmosphere to the change in energy balance as a direct result of the climate driver, and one slower response, scaling with the change in surface temperature (see e.g. [Boucher, 2013; Cao *et al.*, 2012; Kamae and Watanabe, 2012; Myhre *et al.*, 2013a; Sherwood *et al.*, 2015]). The realization that these processes may be very differently represented in models led to the suggestion [Bala *et al.*, 2010] that fast and slow responses be compared separately in multi-model intercomparisons to uncover robust responses in the hydrological cycle. Other publications have noted that the slow precipitation change per degree of warming is well constrained, indicating that the main differences in apparent response lie in the rapid adjustments [Timothy Andrews and Forster, 2010; Fläschner *et al.*, 2016].

Recently, several single model studies have investigated the response to climate drivers in isolation. *Timothy Andrews et al.* [2010] forced the HadGEM1 model with greenhouse gas, aerosol, albedo and solar insolation perturbations. They found strong correlations between the top of atmosphere forcing of a perturbation and the slow, temperature driven precipitation change, and between the modeled atmospheric absorption and the fast precipitation change. *Kvalevåg et al.* [2013] repeated the studies using the NCAR CESM1 model and the CAM4 atmospheric component. They found very similar overall results and correlations to *Andrews et al.* [2010], but a number of significant differences in response to otherwise identical climate perturbations.

No coordinated effort has however yet been made to compare the precipitation response to identical single driver perturbations across a broad range of models. To perform such a comparison was the formative idea behind the Precipitation Driver and Response Model Intercomparison Project (PDRMIP). In the following sections, we present the first results of the PDRMIP effort, based on results reported by nine global climate models. The experiment design broadly follows that used in [*Timothy Andrews and Forster*, 2010] and [*Kvalevåg et al.*, 2013], but with some differences implemented in order to allow as many models as possible to apply identical perturbations to their climate simulations. The details of the PDRMIP setup, aerosol distributions and simulations will be covered in a separate publication. Here, we present the first analysis of the PDRMIP precipitation responses to five climate drivers, and extend the analysis to separate the responses over ocean and various land regions. Upcoming publications will further explore the hydrological sensitivities, energy balances and circulation changes that underlie the present results.

Methods

In PDRMIP, global coupled climate models have performed simulations with comparable configurations, forcing baseline, equilibrated climates with individual drivers. In the following, we define the

perturbations, present the participating models, and show how the temperature, precipitation and radiative forcing responses were calculated. The models used for the present analysis are CanESM2, NorESM1, HadGEM2, HadGEM3-GA4, GISS-E2, NCAR CESM1 CAM4, NCAR CESM1 CAM5, MPI-ESM and MIROC-SPRINTARS. (See Table S1 for details and model references.)

For the present analysis, five perturbations were simulated: A doubling of CO₂ concentration (hereafter denoted *CO2x2*), tripling of CH₄ concentration (*CH4x3*), 2% increase in solar insolation (*Sol+2%*), ten times BC concentration or emissions (*BCx10*) and five times SO₄ concentrations or emissions (*SO4x5*). All perturbations were abrupt, relative to present day or preindustrial values. Greenhouse gas and solar insolation perturbations were applied relative to the models' own baseline values. For the aerosol perturbations, multi-model mean monthly present day concentrations were extracted from the submissions to AeroCom Phase II (see e.g. [Myhre *et al.*, 2013b; Samset *et al.*, 2013]). To form perturbations they were multiplied by the stated factor, and both baseline and perturbed fields were regridded to the native resolution of the PDRMIP models. Some models were however unable to perform simulations with prescribed concentrations. These models instead ran a baseline with present day emissions, and then multiplied these emissions by the prescribed factors.

For the baseline and each perturbation, each model ran two sets of simulations: One keeping sea surface temperatures fixed (hereafter denoted *fSST*), and one with a slab ocean or fully coupled ocean (*coupled*). The *fSST* simulations were run for 15 years, and the *coupled* simulations for 100 years. Only one ensemble member was used for each model. Note that for the present analysis, focusing on sub-centennial responses, the use of a long simulation with constant forcings is equivalent to a perturbed initial-condition ensemble.

Table S1 summarizes the nine models that were used for the present analysis, including their ocean setup and native resolutions, and whether they used emissions or prescribed aerosol concentrations. All

110 models simulated all perturbations, except MPI-ESM which did not have the capability for performing
111 the aerosol perturbations. One model (CESM-CAM4) used a slab ocean setup for the *coupled* simulations,
112 the others used a full ocean representation.

113 Radiative forcing (RF) due to a climate perturbation was diagnosed using use the difference in global
114 mean flux for years 6-15 from the *fSST* simulations. The analysis was performed at top-of-atmosphere
115 (TOA, RF_{TOA}) and at the surface (RF_{surf}). The change in atmospheric absorption due to the climate
116 perturbation was then defined as $Atm.abs. = RF_{TOA} - RF_{surf}$. The run length was determined based on
117 earlier observations that the present models equilibrate well within 5 years of *fSST* running (see e.g.
118 [Kvalevåg *et al.*, 2013]). A Gregory-style regression was also performed [Gregory and Webb, 2008],
119 regressing the global, annual mean flux change relative to the baseline simulation against the change in
120 surface air temperature (ΔTS) in the *coupled* simulations. Both methods yield comparable results – see
121 Supplementary Information.

122 Temperature and precipitation responses to the perturbations were calculated as averages of annual
123 means from the last 10 years of *fSST* simulations, or the last 50 years of the *coupled* simulations. The
124 time windows were chosen to allow both for approximate model equilibration (see Discussion), and to
125 encompass internal annual and decadal variability. For the regional analyses, all modeled precipitation
126 responses were regridded to $1^\circ \times 1^\circ$ resolution.

127 To diagnose the fast precipitation response due to rapid adjustments, ΔP_{fast} , we used the response in the
128 *fSST* simulations. In the coupled simulations, we have assumed that the response over the last 50 years
129 is a linear combination of the fast response and a slow response due to surface temperature change.

130 Hence the slow response can be calculated as $\Delta P_{slow} = \Delta P_{total} - \Delta P_{fast}$.

Results

We first compare the near-surface temperature change and total (fast+slow) precipitation responses to the five climate perturbations, regionally and globally averaged, for all participating models. We then highlight similarities and differences across the multi-model ensemble and for each forcing agent; for RF, fast and slow precipitation responses, and contrasts in behavior between land and ocean.

Figure 1 shows the global mean temperature and precipitation responses to the climate perturbations. For $CO_2 \times 2$, the temperature response varies between about 2-4 K, consistent with the range in modeled climate sensitivities found in CMIP5 [T. Andrews *et al.*, 2012]. We note, however, that most models have not achieved equilibrium 100 years after the perturbation, and hence the full temperature response is likely higher. The precipitation response to $CO_2 \times 2$ ranges from 1-6 %, correlated with the temperature response. The bottom left panel of Figure 1 illustrates this, showing the hydrological sensitivity (HS) for $CO_2 \times 2$ across the models. The HS, defined as $\Delta P_{\text{total}}/\Delta T$ (in recent publications termed the apparent hydrological sensitivity parameter [Fläschner *et al.*, 2016], a terminology which we adopt here) shows much less spread, with a multi-model mean HS of $1.4 \pm 0.3 \text{ \%}/K$ for $CO_2 \times 2$. The error indicates one standard deviation across the present model sample. One model (GISS-E2) stands out as having a markedly lower response than the others, in temperature, precipitation and HS. This is consistent with this model having amongst the lowest equilibrium climate sensitivities of the CMIP5 models [Forster *et al.*, 2013], and being flagged as an outlier in another recent multi-model study investigating CO_2 forcing in CMIP5 [DeAngelis *et al.*, 2015].

For $CH_4 \times 3$ and $Sol+2\%$ the pattern between models is qualitatively similar to $CO_2 \times 2$, although the apparent HS is higher; $1.7 \pm 0.4 \text{ \%}/K$ for $CH_4 \times 3$ and $2.4 \pm 0.2 \text{ \%}/K$ for $Sol+2\%$. This is in line with earlier modelling studies [Allen and Ingram, 2002].

Black carbon shows an opposite precipitation response to the other forcing agents, i.e. it has a negative apparent HS, due to its strong atmospheric absorption of shortwave radiation. All models give a positive temperature response in the *BCx10* case, but with a relatively large spread. The precipitation response is consistently negative, except in one model (HadGEM3-GA4) where it is consistent with zero. The apparent HS for *BCx10* shows sizeable spread.

The sulfate perturbation yields a negative response in both temperature and precipitation, across all models. The HS for *SO4x5* is similar to that for *Sol+2%*, and stronger than for the greenhouse gases. One model (HadGEM3-GA4) finds a markedly strong response to *SO4x5* in both temperature and precipitation, but has a HS in line with the other models. This model version simulates a relatively high sulfate aerosol optical depth per unit mass, and has previously been shown to have a strong indirect aerosol effect relative to comparable models [Wilcox *et al.*, 2015]. NCAR CESM CAM4, which does not include any indirect aerosol effects on clouds, has a sulfate response and a HS that is well within the multi-model spread.

Inspired by earlier single model studies [Timothy Andrews *et al.*, 2010; Kvalevåg *et al.*, 2013], we investigate correlations of precipitation changes with energetic quantities (Figure 2). The left panel shows the regressed change in net atmospheric absorption against the global mean fast precipitation response. RF values were calculated using the fSST method. Figure S1 shows the corresponding results when using 20 year Gregory regressions. As in the previous single model studies, we find a strong negative correlation. The main reason for this is that the greater change in absorption through the atmospheric column, the more convection is suppressed, leading to reduced precipitation and latent heating. All models show atmospheric absorption consistent with zero for *SO4x5* (except one model, CAM5, which calculates 1 W m^{-2}), and around 0.5 W m^{-2} for *CH4x3* and *Sol+2%*. *CO2x2* results in around 2 to 3 W m^{-2} of atmospheric absorption for all models, with a corresponding fast precipitation response of -20 to -40 mm/yr. *BCx10* displays significant absorption in all models, but with a very large range,

from 1 to more than 5 W m^{-2} . The resulting fast precipitation response however largely follows the multi-model, multi-perturbation regression line. Deviations from this regression line can occur because the change in the atmospheric energy budget also depends on changes in surface sensible heat flux, as well as the radiative and latent-heat terms. See e.g. [Fläschner *et al.*, 2016].

The right panel of Figure 2 regresses the change in near-surface temperature (ΔT_S) against the slow precipitation response. We find a strong positive correlation, again in line with previous single model studies. The results for a single driver show a spread in accordance with the climate sensitivities of the PDMIP model sample (generally the same versions as in CMIP5, see [Forster *et al.*, 2013]). For *BCx10* two models (CanESM2, HadGEM2) fall well outside the correlation line, however the temperature change due to the BC perturbation used here is also very low ($<2\text{K}$ for all models). The HadGEM3-GA4 response to *SO4x5* stands out as particularly strong, but still follows the general trend.

Broadly, Figure 2 confirms the physical picture drawn in [Timothy Andrews *et al.*, 2010] and [Kvalevåg *et al.*, 2013]. The precipitation response to a global climate driver can be subdivided into two broad components: A fast response, which scales with changes in the atmospheric absorption, and a slower response related to changes in surface temperature, scaling with the surface temperature change (and, more broadly, TOA RF). Inter-model differences are however significant. The scaling with climate sensitivity in the right panel is far from perfect, and the left panel indicates a wide range of modeled atmospheric absorptions and fast responses for comparable perturbations. Investigating the internal processes that link TOA RF, surface temperature change and atmospheric absorption to precipitation change in these models therefore is a promising way to understand inter-model spread and potentially reduce multi-model uncertainty in precipitation.

Table S2 lists the multi-model average global mean responses to the five perturbations, for radiative forcing, temperature, and total, fast and slow precipitation. The PDRMIP ensemble confirms earlier

model studies indicating a stronger apparent hydrological sensitivity for changes to solar irradiance (2.4 %/K) relative to the greenhouse gases (1.4 %/K). Further, the modeled climates are also more sensitive to aerosol perturbations than to forcing from greenhouse gases, albeit with a significantly higher ensemble uncertainty for *BCx10*. Recent publications have studied how the precipitation response to a climate driver scales with surface temperature change alone, termed the slow hydrological sensitivity (e.g. [Timothy Andrews et al., 2010; Fläschner et al., 2016]), and found that it varies less between models and drivers than the apparent HS. This will be explored for the PDRMIP model ensemble in an upcoming publication.

Figure 3 shows the multi-model mean geographical patterns of the total, fast and slow precipitation responses to the individual perturbations. For most regions and perturbations, the models do not all agree on the sign of the responses, however some robust features are still apparent.

For *CO2x2* (top row), the total response is comprised of a negative fast response at most latitudes, and a stronger positive slow response at all latitudes but with a few exceptions in the inter-tropical convergence (ITCZ) regions. The former is mainly due to the stabilizing effect of the atmospheric absorption of CO_2 , the latter due to the gradual increase in surface temperature. The total precipitation change is strongest around the Equator, dominated by the slow change over the Pacific Ocean. Most regions are dominated by the slow response, but some land regions are dominated by the fast changes. (See below).

CH4x3 and *Sol+2%* (second and third rows) show broadly similar total and slow precipitation response features to *CO2x2*, except that *CH4x3* has lower absolute response due to the weaker RF (as also seen in Figure 1). The model mean fast response to *CH4x3* is non-significant for all latitudes, as expected for climate perturbations with low atmospheric absorption. *SO4x5* (bottom row) shows an inverted pattern to the solar and greenhouse gas perturbations, with virtually no (significant) fast response in the zonal

223 mean. For $CO_2 \times 2$, $CH_4 \times 3$, $Sol + 2\%$ and $SO_4 \times 5$, there is a clear land/ocean difference, in line with earlier
 224 analyses based on the CMIP5 model ensemble [Richardson *et al.*, 2016]. Tropical land areas generally
 225 see a positive fast precipitation response, largely canceled out in the zonal and global means by a
 226 corresponding negative response over tropical oceans.

227 $BC \times 10$ (fourth row) shows a markedly different response pattern to the other perturbations. There is
 228 little slow response, except in the tropics where the zonal mean shows a small positive precipitation
 229 change north of Equator and a smaller negative one south of Equator. The total is dominated by the fast
 230 response, which is generally negative at most latitudes. The aerosol perturbations tend to shift the ITCZ
 231 more (southwards for $SO_4 \times 5$, north for $BC \times 10$) than the solar and GHG changes, due to the more
 232 hemispherically heterogeneous RF that they cause.

233 A common misconception about the change in precipitation caused by a given driver is that it is
 234 composed of an initial, weak fast response due to rapid adjustments, which will over time be
 235 overwhelmed by the slow, temperature driven response. Figure 3, however, indicates that in several
 236 regions, the fast response may dominate even when the climate system approaches a new equilibrium,
 237 in line with what has previously been observed for tropical precipitation under rising CO_2 concentrations
 238 [Bony *et al.*, 2013]. In Figure 4, top row, we explore this by comparing the total, fast and slow
 239 precipitation responses over land and ocean separately, and over six land regions: North America, South
 240 America, Europe, Africa, South Asia and Australia (for region definitions, see Figure S2). There are clearly
 241 large regional and inter-model differences, but some significant features still emerge. Over the ocean,
 242 the climate drivers cause a fast response opposed by a slow response. Over some land regions, however,
 243 the fast and slow responses have the same sign. This signature is particularly clear over South Asia.

244 To determine whether fast or slow precipitation responses dominate over years 51-100 of the PDRMIP
 245 simulations, we define the response ratio $R_{resp} = (|\Delta P_{fast}| - |\Delta P_{slow}|) / (|\Delta P_{fast}| + |\Delta P_{slow}|)$. R_{resp} will be

positive when rapid adjustments dominate the long term precipitation response, and negative when the slow response dominates. For the extreme cases of only fast or slow responses, R_{resp} will be +1 or -1 respectively. The lower panel of Figure 4 shows the multi-model mean R_{resp} for all PDRMIP drivers, for land, ocean and the six regions defined above. For most regions and drivers, the models do not consistently agree on the dominating response (not shown). The response over oceans is, however, consistently dominated by the slow response for all drivers and models, except for *BCx10* where all models but one predict that the fast precipitation response still dominates at near-equilibrium. Considering land regions, South America and Africa are mainly dominated by the fast response for all perturbations. Australia shows a similar pattern, albeit with a much larger intermodel spread. Southeast Asia sees a dominance of the slow response, while North America and Europe have a more mixed response to the different drivers. The latter mainly reflects a large inter-model spread in the results, probably at least partly due to differences in aerosol treatment and lifetime (where emissions were used) for the *BCx10* and *SO4x5* cases. For the *CO2x2* case, one factor likely contributing to the dominance of fast responses over land is the physiological forcing from CO₂-induced stomatal response, which has been shown to significantly affect both surface temperature response and water balance in previous model studies [Cao *et al.*, 2010].

Discussion

Overall, the results presented in the previous section agree with earlier single model studies of the precipitation impacts of individual forcings, and confirm our expectations based on simple energetics. The internal mechanisms linking changes to the energy balance to altered precipitation rates however differ between models, and we do see significant inter-model variability.

The hydrological sensitivity for a *BCx10* perturbation varies strongly between models. One model even shows a positive (non-significant) apparent HS. This is likely due to the multiple ways in which BC can

affect climate – both directly, through absorption and scattering of incoming sunlight, indirectly through modifications of cloud microphysical properties, and semidirectly, through heating ambient air and thus altering stability and/or burning off clouds from within [Bond *et al.*, 2013; Samset and Myhre, 2015]. This range of effects is much larger than e.g. for SO_4x5 , where the additional particles mainly scatter incoming sunlight and affect cloud microphysics. BC–climate interactions are treated very differently in present global climate models, as are transport and removal processes, factors which cause strong variations even for direct radiative forcing (see e.g. [Samset *et al.*, 2013]). E.g. it is interesting to note that the responses for HadGEM2 and HadGEM3-GA4 are markedly different, even though they use the same aerosol physics schemes. Also, some models have used prescribed concentrations based on AeroCom Phase II, and some have used native emissions. As we have not attempted to normalize the responses to the simulated aerosol burden, or to any differences in vertical profile, this is one likely contributor to the observed diversity [Ban-Weiss *et al.*, 2011; Hodnebrog *et al.*, 2014; Samset and Myhre, 2015]. The precipitation response to BC perturbations in PDRMIP will be investigated in detail in a follow-up publication. We note that the differences seen here will have been present for CMIP5, meaning that BC is likely a strong contributor to the prediction diversity seen there.

As noted above, most PDRMIP models ran their *coupled* simulations with a fully coupled ocean. This means that for strong perturbations like CO_2x2 , they will likely not have reached their equilibrium warming within the 100 years simulated here. Recently, Caldeira and Myhrvold [2013] found that in the CMIP5 model ensemble, on average 80% of the equilibrium warming after a $4xCO_2$ perturbation had been realized after the first 100 simulation years. One PDRMIP model (GISS-E2) ran an additional 250 years for our CO_2x2 case, and found an additional 0.5K warming beyond the 1.5K realized over their first 100 years. Another (CanESM2) found an additional 0.6K beyond the 2.7K in the first 100 years when running the model for 800 years. Both of these results are consistent with the Caldeira and Myhrvold [2013] analysis, indicating that we could expect similar extra, long term warming for the other models in

the PDRMIP ensemble. For the present analysis, this non-equilibrium is not crucial for the main conclusions, as models are then well within the regimes where changes to precipitation scale with the slow increase in surface temperature. Hence, for fully equilibrated models both the temperature and precipitation responses to the perturbations would have been stronger, but still follow the trends shown in Figure 2. The ratio of fast to slow precipitation response would however likely change on such long time-scales, changing the regional patterns found in Figures 3 and 4.

A further potential issue with the present analysis is the temperature response over land in the fSST simulations. In principle, the fast response as diagnosed above could have a slow component, as the land surface temperature may increase somewhat with time even if sea surface temperatures are kept constant. We tested the impact of this by calculating the global mean temperature change over land in the fSST case, assuming a resulting precipitation change of $(\Delta P_{\text{slow}} / \Delta T_{\text{land,coupled}}) \times \Delta T_{\text{land,fSST}}$, and reinterpreting it as part of the slow response. While this procedure changes the results by up to 10% for some models, the multi-model mean results presented above are not affected within the uncertainties given.

Conclusions

We have presented the response to perturbations to five climate forcings (*CO2x2*, *CH4x3*, *Sol+2%*, *BCx10* and *SO4x5*) across nine global climate models, as part of the PDRMIP project. As in previous single model studies, we find that global mean precipitation responds on two timescales: One fast response, acting on the timescale of months, that scales closely with the atmospheric energy net absorption due to the forcing agent, and a slower response that scales with the long term change in global surface temperature. All models show broadly similar responses to the perturbations, but beyond this there is still significant inter-model variability, indicating differences in how the atmosphere reacts to altered absorption and surface temperature. Black carbon stands out as the forcing agent with the largest inter-

model spread in hydrological sensitivity. The precipitation response over oceans is quite uniform between models, and dominates the global mean values. Over land, where the precipitation response to climate drivers is arguably much more relevant for human activities, we find large regions where the rapid adjustments dominate over the slow response across the entire model ensemble, even 100 years after the perturbation was applied. The main results in the present paper will be further explored in upcoming PDRMIP publications, with emphasis on hydrological sensitivities, energy balances, circulation changes and radiative forcing.

Acknowledgements

All model results used for the present study are available to the public through the Norwegian NORSTORE data storage facility. BHS, GM and OH were funded by the Research Council of Norway, through the grant NAPEX (229778). Supercomputer facilities were generously provided by NOTUR. DS thanks the NASA High-End Computing Program through the NASA Center for Climate Simulation at Goddard Space Flight Center for computational resources. MK and AV are supported by the Natural Environment Research Council under grant number NE/K500872/1. Simulations with HadGEM3-GA4 were performed using the MONSooN system, a collaborative facility supplied under the Joint Weather and Climate Research Programme, which is a strategic partnership between the Met Office and the Natural Environment Research Council. T. T. was supported by the supercomputer system of the National Institute for Environmental Studies, Japan, the Environment Research and Technology Development Fund (S-12-3) of the Ministry of the Environment, Japan and JSPS KAKENHI Grant Number 15H01728 and 15K12190. DJLO and AK were supported by the Norwegian Research Council through the projects EVA (grant no. 229771) and EarthClim (207711/E10), and NOTUR (nn2345k) and NorStore (ns2345k) projects. TR was supported by NERC training award NE/K007483/1, and acknowledges use of

339 the MONSooN system. Computing resources for JFL ([ark:/85065/d7wd3xhc](https://nvd.nist.gov/vuln/data-feeds#CVE-2019-11461)) were provided by the
340 Climate Simulation Laboratory at NCAR's Computational and Information Systems Laboratory,
341 sponsored by the National Science Foundation and other agencies. Computing resources for the
342 simulations with the MPI model were provided by the German Climate Computing Center (DKRZ),
343 Hamburg.

References

- Allen, M. R., and W. J. Ingram (2002), *Nature*, 419(6903), 224-232
- Andrews, T., and P. M. Forster (2010), *Environ Res Lett*, 5(2), 025212, doi: 10.1088/1748-9326/5/2/025212.
- Andrews, T., J. M. Gregory, M. J. Webb, and K. E. Taylor (2012), *Geophys Res Lett*, 39, doi: Artn L09712
Doi 10.1029/2012gl051607.
- Andrews, T., P. M. Forster, O. Boucher, N. Bellouin, and A. Jones (2010), *Geophys Res Lett*, 37(14), n/a-n/a, doi: 10.1029/2010gl043991.
- Bala, G., K. Caldeira, and R. Nemani (2010), *Climate Dynamics*, 35(2-3), 423-434, doi: 10.1007/s00382-009-0583-y.
- Ban-Weiss, G. A., L. Cao, G. Bala, and K. Caldeira (2011), *Climate Dynamics*, 38(5-6), 897-911, doi: 10.1007/s00382-011-1052-y.
- Bond, T. C., et al. (2013), *Journal of Geophysical Research: Atmospheres*, 118(11), 5380-5552, doi: 10.1002/jgrd.50171.
- Bony, S., G. Bellon, D. Klocke, S. Sherwood, S. Fermepin, and S. Denvil (2013), *Nature Geosci*, 6(6), 447-451, doi: 10.1038/ngeo1799
<http://www.nature.com/ngeo/journal/v6/n6/abs/ngeo1799.html#supplementary-information>.
- Boucher, O., D. Randall, P. Artaxo, C. Bretherton, G. Feingold, P. Forster, V.-M. Kerminen, Y. Kondo, H. Liao, U. Lohmann, P. Rasch, S.K. Satheesh, S. Sherwood, B. Stevens and X.Y. Zhang (2013), Clouds and Aerosols, in *Climate Change 2013: The Physical Science Basis. Contribution of Working Group I to the Fifth Assessment Report of the Intergovernmental Panel on Climate Change*, edited by T. F. Stocker, D. Qin, G.-K. Plattner, M. Tignor, S.K. Allen, J. Boschung, A. Nauels, Y. Xia, V. Bex and P.M. Midgley, pp. 571–658, Cambridge University Press, Cambridge, United Kingdom and New York, NY, USA.

367 Caldeira, K., and N. P. Myhrvold (2013), *Environ Res Lett*, 8(3), 034039

368 Cao, L., G. Bala, and K. Caldeira (2012), *Environ Res Lett*, 7(3), 034015

369 Cao, L., G. Bala, K. Caldeira, R. Nemani, and G. Ban-Weiss (2010), *Proceedings of the National Academy*
370 *of Sciences*, 107(21), 9513-9518, doi: 10.1073/pnas.0913000107.

371 Collins, M., et al. (2013), Long-term Climate Change: Projections, Commitments and Irreversibility, in
372 *Climate Change 2013: The Physical Science Basis. Contribution of Working Group I to the Fifth*
373 *Assessment Report of the Intergovernmental Panel on Climate Change*, edited by T. F. Stocker, D. Qin,
374 G.-K. Plattner, M. Tignor, S.K. Allen, J. Boschung, A. Nauels, Y. Xia, V. Bex and P.M. Midgley, pp. 1029–
375 1136, Cambridge University Press, Cambridge, United Kingdom and New York, NY, USA.

376 DeAngelis, A. M., X. Qu, M. D. Zelinka, and A. Hall (2015), *Nature*, 528(7581), 249-253, doi:
377 10.1038/nature15770.

378 Fläschner, D., T. Mauritsen, and B. Stevens (2016), *J Climate*, 29(2), 801-817, doi: 10.1175/jcli-d-15-
379 0351.1.

380 Forster, P. M., T. Andrews, P. Good, J. M. Gregory, L. S. Jackson, and M. Zelinka (2013), *Journal of*
381 *Geophysical Research: Atmospheres*, 118(3), 1139-1150, doi: 10.1002/jgrd.50174.

382 Gregory, J., and M. Webb (2008), *J Climate*, 21(1), 58-71, doi: 10.1175/2007JCLI1834.1.

383 Hartmann, D. L., A.M.G. Klein Tank, M. Rusticucci, L.V. Alexander, S. Brönnimann, Y. Charabi, F.J.
384 Dentener, E.J. Dlugokencky, D.R. Easterling, A. Kaplan, B.J. Soden, P.W. Thorne, M. Wild and P.M. Zhai
385 (2013), Observations: Atmosphere and Surface, in *Climate Change 2013: The Physical Science Basis.*
386 *Contribution of Working Group I to the Fifth Assessment Report of the Intergovernmental Panel on*
387 *Climate Change*, edited by T. F. Stocker, D. Qin, G.-K. Plattner, M. Tignor, S.K. Allen, J. Boschung, A.
388 Nauels, Y. Xia, V. Bex and P.M. Midgley, pp. 159–254, Cambridge University Press, Cambridge, United
389 Kingdom and New York, NY, USA.

390 Hodnebrog, O., G. Myhre, and B. H. Samset (2014), *Nature communications*, 5, 5065, doi:
 391 10.1038/ncomms6065.
 392 Kamae, Y., and M. Watanabe (2012), *Climate Dynamics*, 41(11-12), 3007-3024, doi: 10.1007/s00382-
 393 012-1555-1.
 394 Knutti, R., and J. Sedláček (2012), *Nat Clim Change*, 3(4), 369-373, doi: 10.1038/nclimate1716.
 395 Kvalevåg, M. M., B. H. Samset, and G. Myhre (2013), *Geophys Res Lett*, 40(7), 1432-1438, doi:
 396 10.1002/grl.50318.
 397 Myhre, G., et al. (2013a), Anthropogenic and Natural Radiative Forcing, in *Climate Change 2013: The*
 398 *Physical Science Basis. Contribution of Working Group I to the Fifth Assessment Report of the*
 399 *Intergovernmental Panel on Climate Change*, edited by T. F. Stocker, D. Qin, G.-K. Plattner, M. Tignor, S.K.
 400 Allen, J. Boschung, A. Nauels, Y. Xia, V. Bex and P.M. Midgley, pp. 659–740, Cambridge University Press,
 401 Cambridge, United Kingdom and New York, NY, USA.
 402 Myhre, G., et al. (2013b), *Atmos Chem Phys*, 13(4), 1853-1877, doi: DOI 10.5194/acp-13-1853-2013.
 403 O’Gorman, P., R. Allan, M. Byrne, and M. Previdi (2012), *Surv Geophys*, 33(3-4), 585-608, doi:
 404 10.1007/s10712-011-9159-6.
 405 Richardson, T. B., P. M. Forster, T. Andrews, and D. J. Parker (2016), *J Climate*, 29(2), 583-594, doi:
 406 10.1175/jcli-d-15-0174.1.
 407 Samset, B. H., and G. Myhre (2015), *Journal of Geophysical Research: Atmospheres*, 120(7), 2913-2927,
 408 doi: 10.1002/2014JD022849.
 409 Samset, B. H., et al. (2013), *Atmos Chem Phys*, 13(5), 2423-2434, doi: DOI 10.5194/acp-13-2423-2013.
 410 Sherwood, S. C., S. Bony, O. Boucher, C. Bretherton, P. M. Forster, J. M. Gregory, and B. Stevens (2015),
 411 *B Am Meteorol Soc*, 96(2), 217-228, doi: 10.1175/bams-d-13-00167.1.
 412 Wilcox, L. J., E. J. Highwood, B. B. B. Booth, and K. S. Carslaw (2015), *Geophys Res Lett*, 42(5), 1568-1575,
 413 doi: 10.1002/2015GL063301.

Figures

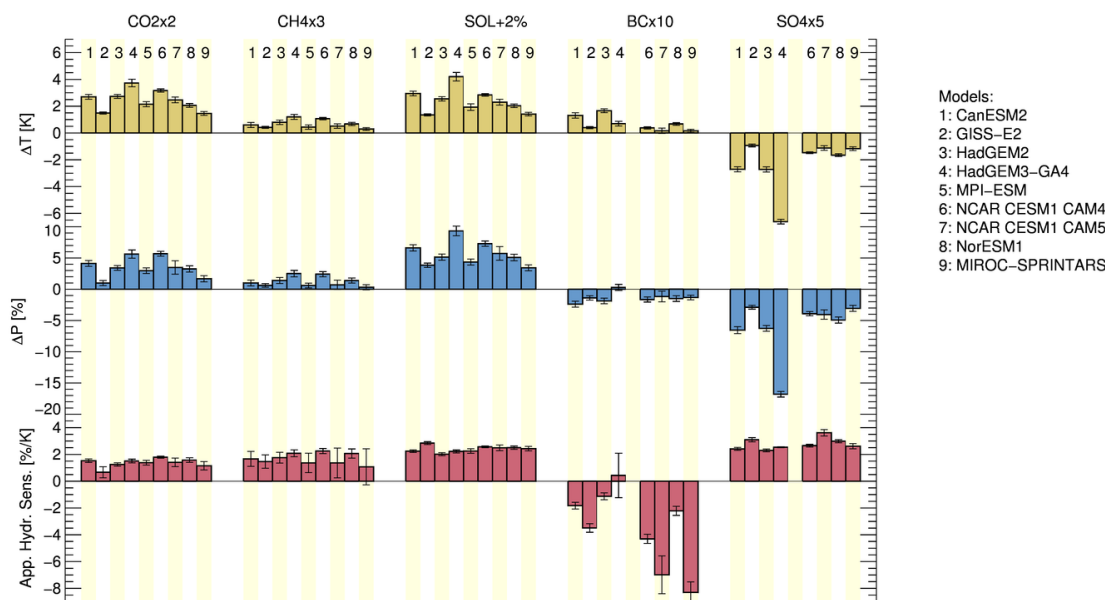


Figure 1: Global, annual mean temperature (top row) and precipitation (middle) change for years 51-100 following a climate perturbation, and the resulting apparent hydrological sensitivity. The numbers indicate the participating models. Error bars indicate \pm one standard deviation of interannual variability.

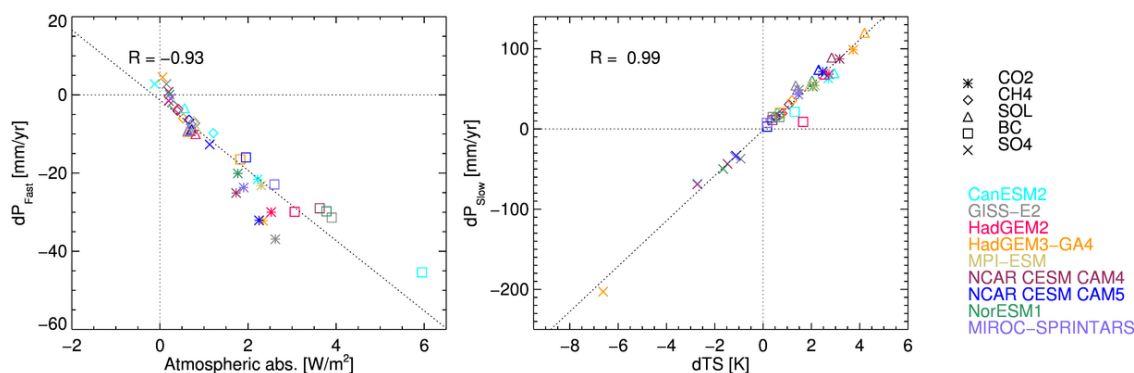
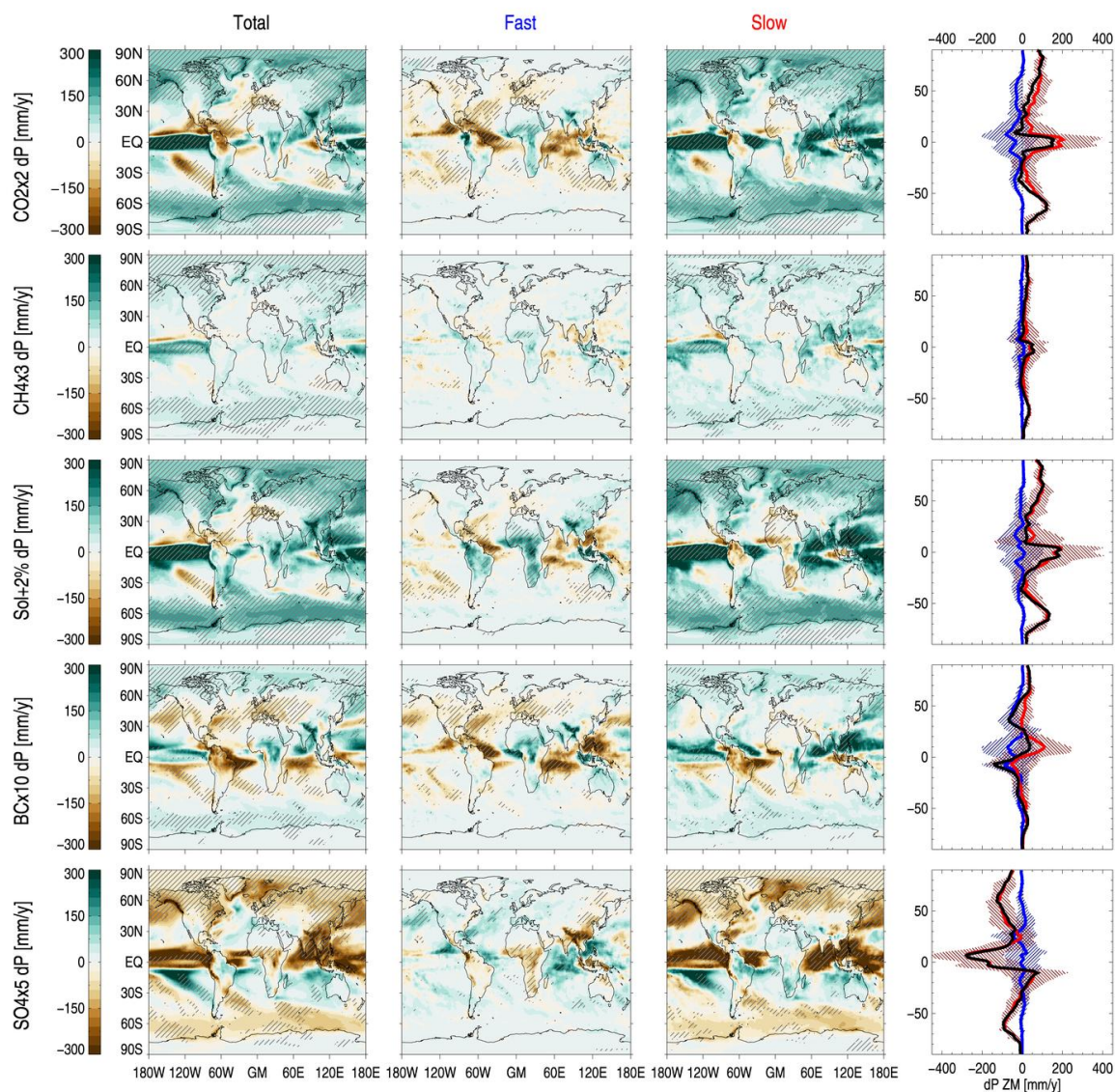


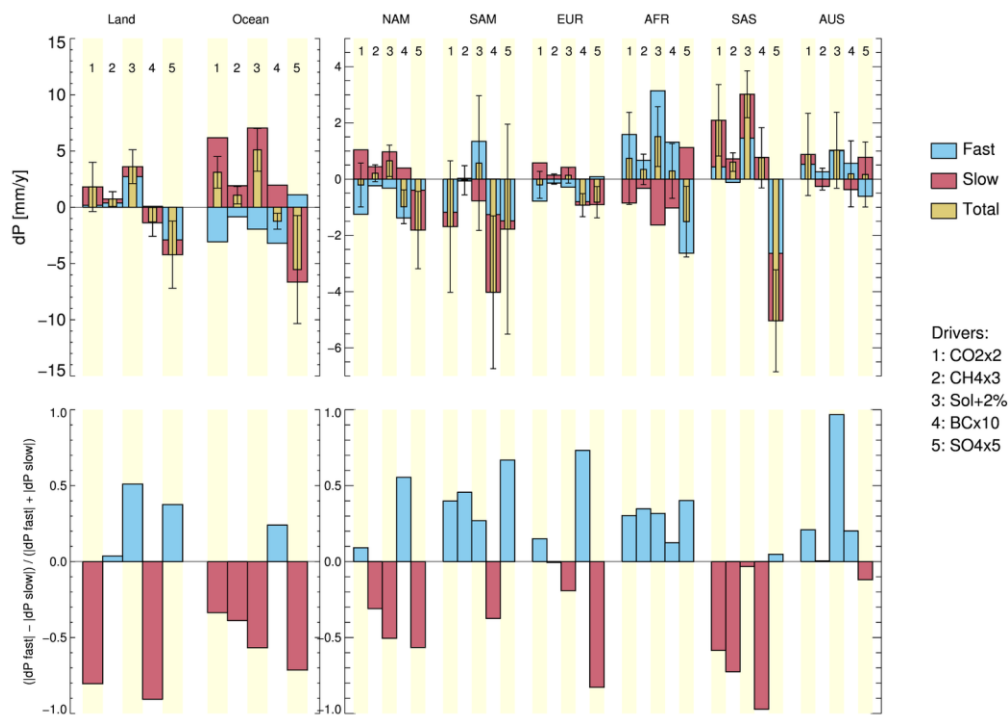
Figure 2: Regression of fast precipitation change vs. atmospheric absorption (left) and slow precipitation change vs. top-of-atmosphere radiative forcing (right). The shown regression lines and Pearson coefficients of correlation (R) are for the combined data from all models and climate perturbations.



425 *Figure 3: Geographical patterns of multi-model mean precipitation change. Each row shows a different*
 426 *climate perturbation. Hatched regions indicate where the multi-model mean is more than one standard*
 427 *deviation away from zero. Left map column: Total change. Center map column: Fast change due to rapid*
 428 *adjustments. Right map column: Slow change due to surface temperature change. Rightmost column:*

429 Multi-model zonal means, showing fast (blue), slow (red) and total (black) precipitation changes. The
 430 shaded bands show $\pm 1\sigma$ of the 9-model ensemble.

431



432

433 Figure 4: Top row: Regional precipitation response, divided into fast and slow components for 5 climate
 434 drivers. The left panel shows the land and ocean responses separately. The right panel shows the response
 435 for the land-only regions of North America (NAM), South America (SAM), Europe (EUR), Africa (AFR), the
 436 major aerosol emission regions of South Asia (SAS), and Australia (AUS). See Figure S2 for definitions.
 437 Bottom row: Response ratio (see text), calculated from the multi-model mean values in the top row.

438